ACS OMEGA

http://pubs.acs.org/journal/acsodf

Article

Synthesis of Chainlike ZSM-5 with a Polyelectrolyte as a Second Template for Oleic Acid and Ethanol Cracking into Light Olefins

Wen He, Fuwei Li, Yufei Gu, Xiaofeng Wang, Hengshuo Gu, Hongbing Fu, Xiumei Liang, and Zhixia Li*

Cite This: *ACS Omega* 2022, 7, 40520−40531

Read Online

ACCESS | Metrics & More | Article Recommendations | Supporting Information

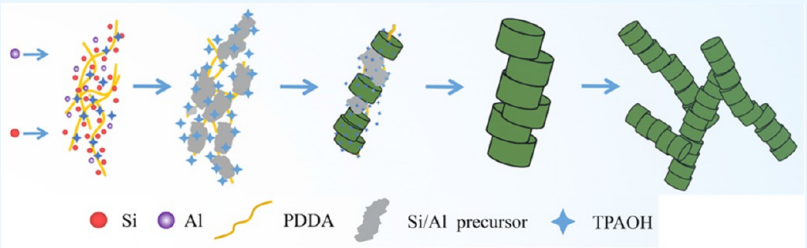

ABSTRACT: Chainlike ZSM-5 was synthesized in a tetrapropylammonium hydroxide (TPAOH) and poly(diallydimethylammonium chloride) (PDDA) dual-template system. The synthesis parameters and formation mechanism of chainlike zeolites were investigated. The optimized composition of the synthesis mixture was as follows: the PDDA/SiO_2, TPAOH/SiO_2, SiO_2/Al_2O_3, and H_2O/SiO_2 molar ratios are, respectively, 0.16, 0.4, 50, and 40, with tetraethyl orthosilicate and aluminum nitrate as silicon/aluminum sources. The resultant ZSM-5 showed a cross-linked chainlike morphology, mesopore-dominated pore structure, and mild acidity. The formation of the chainlike zeolite was attributed to synergistic actions between PDDA and TPAOH. TPAOH acted as an alkali source and helped to induce nucleation and control the crystal size. PDDA acted as a soft template to promote crystal nucleation, and a hard template to form a three-dimensional mesoporous structure. Light olefin ($C_{2-4}^{=}$) selectivities from cracking of ethanol and oleic acid over the present chainlike ZSM-5 at 400 °C reached 90 and 75.7%, respectively, which were much higher than those from commercial ZSM-5 (75 and 52.3%, respectively), demonstrating the excellent hydrothermal stability and catalytic performance of the synthesized chainlike zeolite.

1. INTRODUCTION

ZSM-5 has been widely used in petrochemical engineering as an adsorbent and a catalyst on account of its novel properties, which include a large surface area, excellent hydrothermal stability, unique microporous structure, and controllable acidity.[1,2] However, the small pores of ZSM-5 (0.5−0.6 nm) tend to cause severe diffusion restriction, especially for macromolecular feeds. Significant effort has been made to develop mesoporous zeolites that could overcome the shortcomings of ZSM-5.[3−6] Common methods for the production of mesopores in zeolites include the introduction of hard templates (e.g., carbon nanoparticles, polymer beads, and nanosized $CaCO_3$) or soft templates (e.g., cetyltrimethylammonium bromide, dimethyloctadecyl[3-(trimethoxysilyl)propyl]ammonium chloride, and organosilanes) to the crystallization process of aluminosilicate gels.[7,8] However, hard templates tend to produce isolated pores, which are short of tunnels, consequently limiting mass transfer. Soft template-mediated molecular sieves, such as MCM-41, demonstrate distinct and regular mesoporous structures but feature low acidity and insufficient thermal stability,[9,10] which are unfavorable for cracking reactions at elevated temperatures. Besides, soft templates are expensive and generally commercially unavailable; as such, their industrial applications are limited.[11] Therefore, designing new strategies to fabricate zeolites with controlled acidity and network mesoporous structures is of great importance for the development of new catalysts for catalytic cracking.

Several research groups have recently reported a novel method to obtain chainlike zeolites by coupling the crystallization and self-assembly of individual crystals.[12−17] The resultant zeolites exhibited excellent mechanical strength, macroporosity, and improved acidity and thermal stability, thereby indicating the great application potential of the method to shape-selective catalysis, especially for the FCC of bulky molecular feeds. Aoki et al. synthesized chainlike silicalite via the hydrothermal treatment of a mixture of tetraethyl orthosilicate (TEOS) and tetrapropylammonium hydroxide (TPAOH) in the presence or absence of poly(diallydimethylammonium chloride) (PDDA).[12] They found

Received: September 5, 2022
Accepted: October 19, 2022
Published: October 28, 2022

https://doi.org/10.1021/acsomega.2c05763
ACS Omega 2022, 7, 40520−40531

that linear chainlike superstructures were only obtained in the presence of PDDA. The authors surmised that positively charged PDDA could combine with negatively charged silicate particles to form PDDA/silicate hybrid conjugates, which are subsequently adsorbed onto developing silicate (010) crystal surfaces to induce the cross-linking of neighboring crystals via silanol condensation. Chainlike ZSM-5 has been fabricated using a similar method.[13] The obtained ZSM-5 had strong acidity and showed much higher conversion rates during 1,3,5-triisopropylbenzene cracking compared with conventional ZSM-5.

Chainlike zeolites have been obtained using sucrose[14] and sodium alginate[15] as co-templates instead of PDDA. Carboxyl and hydroxyl groups derived from the co-templates could synergistically induce the formation of a chainlike morphology. Quan et al. synthesized chainlike ZSM-5 using TPAOH as the sole template agent and found that in the absence of other organic additives, a chain morphology could only be obtained over a narrow TPAOH/Si ratio (i.e., 0.3−0.5).[16] In another study, the vapor treatment of TPAOH-coated SiO_2@bacterial cellulose scaffolds resulted in three-dimensional oriented stacking superstructures.[17] The authors thus believed that TPAOH induces nucleation and mediates the crystal morphology, leading to the oriented assembly of MFI crystals; bacterial cellulose then holds the oriented assembly together, thereby forming three-dimensional superstructures.

The above studies suggest that PDDA and TPAOH play a key role in controlling the morphology of chainlike zeolites. PDDA and TPAOH are similarly positively charged, which means both templates could generate strong interactions toward negatively charged aluminosilicate particles. Both templates also contain alkyl regions in their chemical structure, which indicates that they can decrease the surface tension of developing crystals after adsorption on the crystal surface. Differences in their chemical structure (e.g., charge strength and length of the alkyl group) may endow PDDA and TPAOH with different structure-directing abilities. However, how the synergistic effect between PDDA and TPAOH could accurately control the chainlike morphology of the resultant material during the hydrothermal synthesis of zeolites is incompletely understood. In the present work, the influence of various synthesis parameters, such as the amounts of the templates (PDDA, TPAOH), SiO_2/Al_2O_3 ratio, the types of silicon/aluminum sources, and the concentration of raw materials, on the morphology of zeolites was investigated. The formation mechanism of zeolites with a chainlike morphology was also studied. Finally, the catalytic performance of the zeolites was investigated via the cracking of bio-based feeds (i.e., oleic acid and ethanol) to produce light olefins.

2. MATERIALS AND METHODS

2.1. Materials. Tetrapropylammonium hydroxide (TPAOH, 25% in water, Macklin Chemical Reagent), tetraethyl orthosilicate (TEOS, 98%, Sinopharm Chemical Reagent Co., Ltd.), aluminum nitrate nonahydrate (ANI, 99%, Guanghua Chemical Reagent Co., Ltd.), polydiallyldimethylammonium chloride (PDDA, molecular weight = 10−20 × 10^4, 20%, Aladdin Reagents) were used as received. Commercial HZSM-5 (SiO_2/Al_2O_3 = 50) was supplied by Nankai University Catalyst Corporation (Tianjin, China).

2.2. Preparation of the Catalysts. The ZSM-5 zeolites were synthesized via the hydrothermal method with TEOS as the silicon resource, ANI as the aluminum source, and TPAOH and PDDA as co-templates. The morphologies of the zeolites were controlled by adjusting the molar ratios of PDDA/SiO_2 (x), TPAOH/SiO_2 (y), SiO_2/Al_2O_3 (z), and H_2O/SiO_2 (m) in the synthesis mixture. The molar number of PDDA was calculated on the basis of the number of nitrogen atoms in the polymer. In a typical synthesis run, the molar composition of the synthesis mixture was set as 1 SiO_2:0.4 TPAOH:40 H_2O:0.02 Al_2O_3:0.16 PDDA, that is, x = 0.16, y = 0.4, z = 50, and m = 40. The synthesis procedure was as follows: 14 g of TEOS was dropped into an aqueous solution containing 50 g of H_2O, 17 g of TPAOH, and 9 g of PDDA at a constant speed (finish dropping in 5 h at room temperature); 0.51 g of ANI was beforehand dissolved in 5 g of TPAOH aqueous solution and then added to the above silica-containing mixture, which was further stirred for 5 h at a speed of 200 rpm. As the amount of TEOS added increased, PDDA gradually precipitated to form a spherical aggregate, likely because the ethanol released from TEOS hydrolysis decreases the solubility of PDDA.[18,19] The spherical PDDA aggregate (1−2 cm in diameter) was removed by tweezers, and the remaining suspensoid was transferred into a crystallization kettle and reacted at 180 °C for 48 h. The obtained solid product was filtered, washed with distilled water, and then dried overnight at 105 °C. Afterward, the product was calcined at 550 °C for 6 h. The obtained sample was ion-exchanged twice in NH_4Cl solution (1 M, m(liquid)/m(solid) = 10) under stirring at 90 °C for 4 h. The obtained solid sample was calcined at 550 °C for 6 h to obtain HZSM-5, which was denoted CZ-5. CZ-5 was tableted, granulated, and sieved to obtain 20−30-mesh catalysts for the further catalytic reaction.

2.3. Characterization of the Catalysts. The composition of the zeolites was analyzed by X-ray diffraction (XRD, Agilent SmartLab3). The surface morphology of the zeolites was observed with a field emission scanning electron microscope (FESEM, Hitachi SU8220) and a scanning electron microscope (SEM, Hitachi S-3400N). Crystal growth was observed by a transmission electron microscope (TEM, FEI Talos F200X). The ζ potential and size of sol particles during synthesis were measured with a NanoBrook Omni instrument. The size of the sol particles was determined in dynamic light scattering (DLS) mode.

The acidity of the zeolites was analyzed via the temperature-programmed desorption of NH_3 (NH_3-TPD), which was performed on an AMI-300Lite chemisorption apparatus. The catalyst sample (100 mg) was loaded and activated at 550 °C under an Ar flow for 0.5 h and then cooled to 100 °C. A stream of gaseous ammonia (8 vol % in He, 30 mL/min) was introduced to saturate the sample for 40 min. The sample was then flushed with He (20 mL/min) for 60 min. NH_3 desorption was initiated by heating from 100 to 600 °C at a rate of 10 °C/min. A thermal conductivity detector was used to monitor the desorbed NH_3. The ammonia pulse quantitative method was used to calculate the total acid content of the samples. Gauss software was used to fit the obtained NH_3-TPD curve and analyze the acid strength distribution. The acid types of samples were analyzed by pyridine adsorption infrared spectra (Py-IR) on a Fourier transform infrared spectrometer (Thermo Nicolet 6700).

The solid-state magic angle spinning (MAS) nuclear magnetic resonance (NMR) spectra of ^{27}Al were collected on a Bruker AVWBIII 600 MHz NMR spectrometer at a spinning rate of 13 kHz with a $\pi/12$ pulse width of 0.4 μs and a

https://doi.org/10.1021/acsomega.2c05763
ACS Omega 2022, 7, 40520−40531

recycle delay of 1 s by scanning 10 000 times; the probe diameter was 3.2 mm.

N_2 adsorption−desorption isotherms at −196 °C were determined with a Quantachrome NOVA 2200e instrument. The total pore volume (V_{total}), micropore volume (V_{micro}), mesopore volume (V_{meso}), and external surface area (S_{ext}) of the catalysts were measured according to a previously reported method.[20] The pore size distribution of the catalyst was obtained using the nonlocal density functional theory model.

2.4. Catalytic Cracking Tests. The catalytic cracking experiments were performed in a fixed-bed quartz tube reactor (inner diameter, 10 mm; length, 400 mm). Long-chain oleic acid and small-molecule ethanol were selected as raw materials for the cracking tests because both materials are renewable resources. Oleic acid cracking was conducted by loading the catalyst (0.3 g) into the reactor and heating it to 400 °C under a N_2 stream (flow rate, 40 mL/min). Oleic acid (1.0 mL) was slowly injected into the reactor by a syringe pump with a weight hourly space velocity (WHSV) of 6 h^{-1}. The reaction products were cooled to −10 °C. The obtained gas was collected into a gas collection bag, and the volume was recorded. The gas products were analyzed using a gas chromatograph (GC, FULI-9790II, China) equipped with a flame ionization detector and an HP-PLOT/Q capillary column. The carbon deposits on the catalysts were analyzed using a thermogravimetric analyzer (DTG-60H) with an air flow of 20 mL/min and a temperature ramp rate of 10 °C/min from room temperature to 800 °C.

Ethanol cracking was achieved by continuously injecting ethanol into the reactor and reacting for 5 h under the same temperature and WHSV conditions. The gas products were collected every 30 min.

The yields of total gas production (Y_{TGP}) and light olefins (Y_{LO}) and the selectivity to light olefins (S_{LO}) were calculated by using the following equations

$$Y_{TGP}(mL/g) = V_{TGP}/M_0 \times 100\% \quad (1)$$

$$S_{LO}(\%) = x(C_2H_4) + x(C_3H_6) + x(C_4H_8) \quad (2)$$

$$Y_{LO}(mL/g) = Y_{TGP} \times S_{LO} \quad (3)$$

where V_{TGP} is the total volume of the gas product excluding N_2 (mL), x is the molar percentage of light olefins in the gas product (%), and M_0 is the mass of the raw materials (g).

3. RESULTS AND DISCUSSION

3.1. Optimization of the Synthesis Parameters. *3.1.1. PDDA/SiO_2 Molar Ratio.* The amount of PDDA added to the reaction system can change the charge of the gel mixture and affect crystal nucleation. Zeolites with different PDDA/SiO_2 ratios (x = 0−0.16) were synthesized with a TPAOH/SiO_2 ratio (y) of 0.4, a SiO_2/Al_2O_3 ratio (z) of 50, and a H_2O/SiO_2 ratio (m) of 40. Interestingly, while no PDDA was used, excellent isolated near-spherical crystals with a diameter of ∼300 nm were formed (Figure 1a), thus reflecting the strong ability of TPAOH to induce nucleation. A PDDA/SiO_2 ratio of 0.09 led to the formation of a large number of short chains with lengths of ∼1.0 μm. When x was 0.16, the length of single chains increased to ∼2.5 μm, and a large number of cross-linked chains were produced. The amount of PDDA clearly had a significant effect on the morphology of the resultant zeolites. A PDDA/SiO_2 ratio of 0.09−0.16 appeared to be suitable for generating a chainlike morphology. As the amount

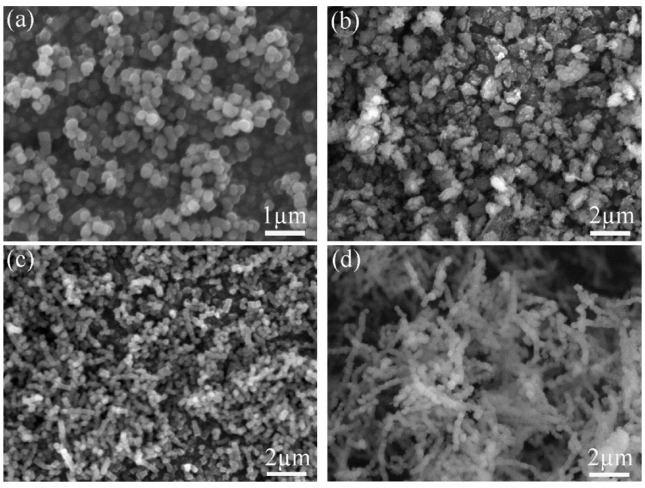

Figure 1. SEM images of zeolites synthesized with different PDDA/SiO_2 molar ratios (x): (a) 0, (b) 0.02, (c) 0.09, and (d) 0.16.

of PDDA increased, the molecules agglomerated into twos and threes.[19,21] Negatively charged silica−alumina gel particles could be adsorbed and nucleate along the three-dimensional structure of PDDA agglomerates, eventually increasing in size to form a cross-linked chain structure.

3.1.2. TPAOH/SiO_2 Molar Ratio. TPAOH releases OH^- and TPA^+ during synthesis and, thus, acts as an alkali source and a template.[22] The role of TPAOH was examined by changing the TPAOH/SiO_2 ratio (y) from 0.2 to 0.6 with x = 0.16, z = 50, and m = 40. As shown in Figure 2, no regular crystal was formed at y = 0.2. When y was increased to 0.3, large disclike crystals with diameters of 2−3 μm were produced. Large numbers of long and cross-linked chains were formed when y was increased to 0.4. The chains became shorter and the single crystals became smaller with a further increase in y.

Compared with PDDA, TPAOH clearly plays a more critical role in controlling the degree of nucleation and morphology of crystals. However, the amount of TPAOH added to the reaction system must be accurately restricted to produce long chains and cross-linked chain network structures. Previous research indicated that the proper TPAOH/SiO_2 ratio is 0.3−0.5. At a lower y value, the hydrolysis rate of aluminosilicate gel and the number of nuclei generated decrease, leading to the formation of amorphous materials and larger crystals. Excess TPAOH releases large amounts of TPA^+ and OH^-, which, in turn, accelerate the hydrolysis of silicon/aluminum sources and the nucleation rate; in this case, the number of nuclei increases and smaller crystals are produced.[19,22] At a proper TPAOH/SiO_2 ratio of 0.4, the hydrolysis rate of the silicon/aluminum sources and the number of nuclei generated could be precisely controlled so that uniform crystals with appropriate dimensions and smooth surfaces are produced. Moreover, crystal nucleation and growth occur more easily around PDDA agglomerates because of the strong electrostatic attraction of the latter. These create favorable conditions for the stacking of adjacent crystals to form a chainlike morphology.

Although it is not clear how cationic polymers or TPAOH induce the stacking of crystals under synthesis conditions, it was generally considered to be associated with the change of interface surface tension.[23] The existence of alkyl parts in the polymers and TPAOH indeed cause a decrease in the interface surface tension. Hydroxyls and silanols are believed to be the reactive species that could cross-link adjacent crystals via

https://doi.org/10.1021/acsomega.2c05763
ACS Omega 2022, 7, 40520−40531

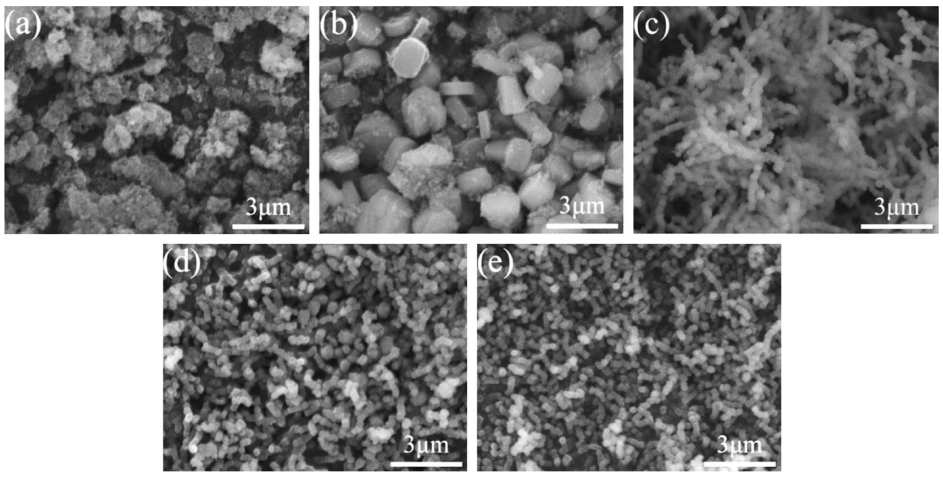

Figure 2. SEM images of zeolites with different TPAOH/SiO_2 ratios (y): (a) 0.2, (b) 0.3, (c) 0.4, (d) 0.5, and (e) 0.6.

condensation.[12,16] Thus, we assume that soluble PDDA or TPAOH could combine with aluminosilicate particles to produce PDDA/aluminosilicates or TPAOH/aluminosilicate electrostatic conjugates, which are absorbed onto the certain crystal faces of the developing zeolites. Such adsorption not only reduces the surface energy but also presents reactive species (e.g., Si−OH, Al−OH). Neighboring crystals are closely connected via the condensation of surface reactive groups between crystals.

3.1.3. SiO_2/Al_2O_3 Molar Ratio. The appropriate acidity is necessary for zeolite catalysts in most reactions, and the acidity of zeolites is commonly dependent on the SiO_2/Al_2O_3 ratio. The effect of the SiO_2/Al_2O_3 ratio (z) on the morphology of zeolites was investigated under the conditions of x = 0.16, y = 0.4, and m = 40 to expand the applications of chainlike zeolites. As shown in Figure 3, the particle size of single crystals

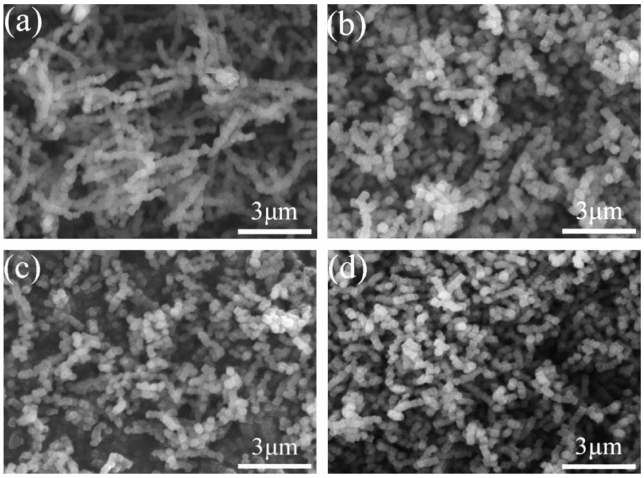

Figure 3. SEM images of zeolite samples obtained from the synthesis mixture with different SiO_2/Al_2O_3 ratios (z): (a) 50, (b) 100, (c) 300, and (d) ∞.

appeared to show no change at different z, but the length of single chains and the cross-linking degree between chains decreased significantly with increasing z. Obtaining long-chain zeolites at a SiO_2/Al_2O_3 ratio > 100 is quite difficult, as reported by Quan et al.[16] We speculate that compared with Si−OH, Al−OH could more easily combine with soluble PDDA and be adsorbed on certain crystal surfaces, which facilitates interlinking between crystals via the condensation of Al−OH and Si−OH. The hydrolysis of the aluminum source (ANI) also consumes a certain amount of TPAOH, and the remained TPAOH concentration in the mixture would be moderate for forming long chains and cross-linked chain structures via controlling the hydrolysis rate of silicon/aluminum sources and the number of crystal nuclei generated, as proposed in previous sections.

Different silicon/aluminum sources were used to synthesize zeolites to reveal the relevant reaction mechanism. As illustrated in Figure S1, a chainlike stacked morphology could be formed from TMOS but not from other silicon sources (e.g., silica sol, silica, and fumed silica). TMOS and TEOS can produce small-molecule alcohols and silanol during hydrolysis, and these alcohols may modify the nuclei and crystals to form abundant hydroxyl groups. Hydroxyl and silanol groups are considered reactive species that could cross-link adjacent crystals via condensation.[12,16]

As shown in Figure S2, chainlike zeolites could be obtained from aluminum isopropoxide ($C_9H_{21}AlO_3$), $Al_2(SO_4)_3{\cdot}18H_2O$, and $AlCl_3{\cdot}6H_2O$ but not $NaAlO_2$ as aluminum sources. This finding suggests that Na^+ in $NaAlO_2$ could restrain the formation of a chainlike morphology.

3.1.4. H_2O/SiO_2 Molar Ratio. The amount of water added to the reaction system directly influences the concentration of all components and affects the particle size and morphology of the end products. Zeolites with different H_2O/SiO_2 ratios (m) were synthesized under the optimized conditions of x = 0.16, y = 0.4, and z = 50. As shown in Figure 4, long chains and cross-linked chain structures could clearly be observed when m values are 30 and 40. The chains became shorter and the cross-linking degree decreased when m exceeded 45. The particle size of individual crystals obviously increased at m = 50. These results reveal that the amount of water added to the reaction system significantly affects the formation of chainlike structures. Increases in water reduce the concentration of all reactants and the charge density of the synthesis mixture, thereby retarding crystal nucleus formation but accelerating crystal growth.[24,25]

According to the results described above, the composition of the synthesis mixture significantly influences the morphology of the resultant zeolites. Chainlike ZSM-5 zeolites can be produced via the synergistic effects of PDDA and TPAOH

https://doi.org/10.1021/acsomega.2c05763
ACS Omega 2022, 7, 40520−40531

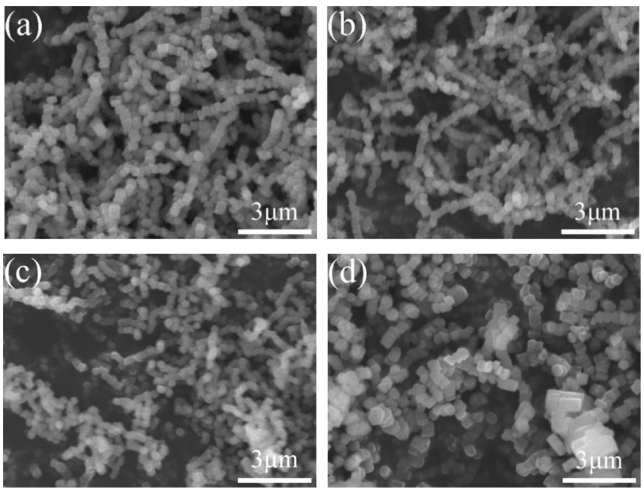

Figure 4. SEM images of the zeolites obtained from the synthesis mixture with different H_2O/SiO_2 (m) ratios: (a) 30, (b) 40, (c) 45, and (d) 50.

with the appropriate raw material ratios as follows: TEOS as the silicon source, ANI as the aluminum source, and PDDA/SiO_2, TPAOH/SiO_2, SiO_2/Al_2O_3, and H_2O/SiO_2 molar ratios of 0.16, 0.4, 50, and 40, respectively. The chain length and cross-linking degree could be well controlled by adjusting these parameters.

3.2. Characterization of the Zeolite. *3.2.1. Composition and Morphology.* The XRD pattern of zeolites synthesized under the optimized conditions of $x = 0.16$, $y = 0.4$, $z = 50$, and $m = 40$ (CZ-5) is shown in Figure 5. Several typical diffraction peaks at 2θ of 7.97, 8.90, 23.1, 23.97, and 24.43° were observed, and these peaks were, respectively, ascribed to the 101, 200, 051, 303, and 133 reflections of the MFI zeolite (PDF-37-0359).[26] The FESEM images show that single chains with a chain length of ~3.5 μm could be formed by the stacking of approximately 20 individual disclike crystals along the b-axis direction. Cross-linking between chains clearly occurred. The outer surfaces of the chains showed deep gully-like folds along the b-axis direction, while the interface between two adjacent crystals was relatively flat and smooth. The relatively flat surface of the (010) plane creates favorable conditions for sticking crystals to form a chainlike structure.[16]

The TEM images in Figure 6a show that some short chains are connected at the sides of long chains to form a cross-linked chain structure. Some overlap occurred at the interface of the adjacent crystals, as indicated by the gray areas (Figure 6b), which correspond to the misplaced stacked interface, as indicated in Figure 5d. The overlapping gray areas suggest that the crystals continuously grow along both directions (i.e., the b-axis direction and the direction perpendicular to the b-axis) even after stacking to form chains. As a result, the diameters of the crystals increased, and the 010 faces exposed by the misplaced stacking of crystals continuously grew along the b-axis. The selected area electron diffraction (SAED) pattern shown in Figure 6c indicates that the selected areas belong to a single-crystal structure. Clear lattice fringes were observed at the interface between the adjacent crystals in Figure 6d, and the interface lattice fringes were in the same direction as those in adjacent crystals, thereby indicating tight connections between adjacent crystals. Lattice fringes of approximately 1.10 nm were assigned to the (101) lattice plane of the crystals, which indicates that the obtained crystals are aligned in an orderly manner along the b-axis direction parallel to the chain axis.[27] Obviously, these chainlike zeolites tend to produce long straight channels in the b-axis direction and expose more zigzag channels in the a-axis direction of chains.

3.2.2. Acidity. The NH_3-TPD profiles of CZ-5 are illustrated in Figure 7a and compared with those of commercial ZSM-5 (Commer-Z-5). Two separate NH_3 desorption peaks were observed in the TPD curves of both zeolites. The amounts of weak and strong acids were calculated from the peak areas in the temperature range of 100−300 °C and above 300 °C, respectively,[28] and the results are listed in Table 1. The amounts of total acids and strong acid sites of CZ-5 were much lower than those of Commer-Z-5; thus, the former is less acidic than the latter. Some researchers reported the limitations of the NH_3-TPD method for measuring Brønsted site densities and the strength of the acidity of zeolites.[29] They thought that peak temperatures in TPD from high-surface-area materials are

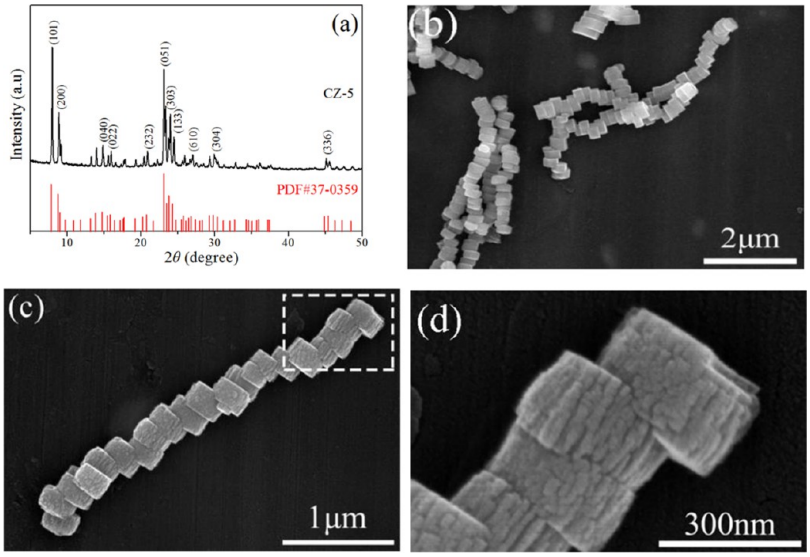

Figure 5. Chainlike ZSM-5 zeolite obtained from the synthesis mixture with the composition: $x = 0.16$, $y = 0.4$, $z = 50$, and $m = 40$. (a) XRD pattern; (b) FESEM image; (c) FESEM image of a single chain; and (d) FESEM image of the selected area in c.

https://doi.org/10.1021/acsomega.2c05763
ACS Omega 2022, 7, 40520−40531

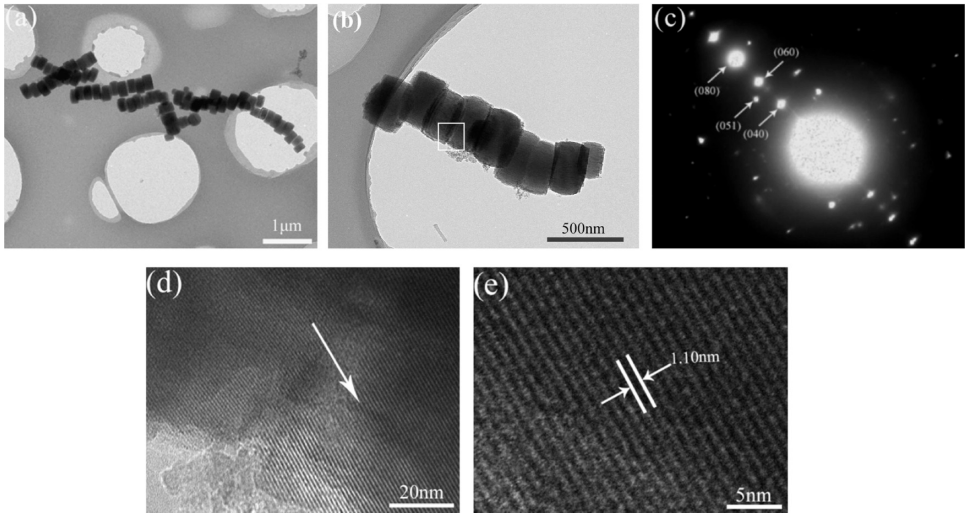

Figure 6. (a) TEM image of chains; (b) TEM image of a single chain; (c) the corresponding SAED pattern viewed along the crystallographic (−4,0,0) axis showing (040), (060), and (080) reflections with the corresponding d-spacings of 0.50, 0.34, and 0.25 nm, respectively. The (051) reflection, 9.3° to the *b*-axis, was used as a reference; (d) lattice fringes at the interface between the adjacent crystals; and (e) high resolution transmission electron microscopy (HRTEM) image of the selected area.

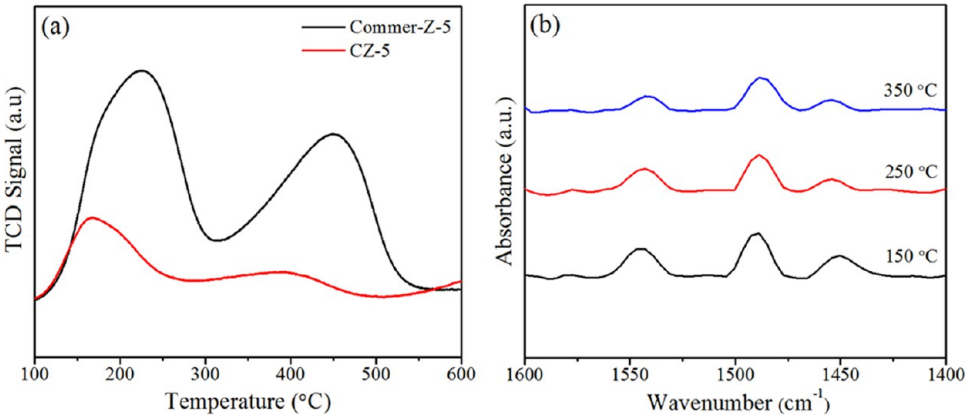

Figure 7. NH_3-TPD profiles (a) and Py-IR spectra (b) of zeolites.

Table 1. Acidity Properties of CZ-5 and Commer-Z-5 from NH_3-TPD Analysis

		percentage of acid sites in total acidity (%)		
catalysts	total acid (μm/g)	weak acid	strong acid	strong/weak
CZ-5	260.4	65.15	34.85	0.53
Commer-Z-5	1152.1	53.08	46.92	0.88

not a simple function of adsorption strength, and NH_3 can be adsorbed on almost all surfaces, not just Brønsted sites. Therefore, the acidity of catalyst samples should be analyzed by combining other methods, e.g., pyridine IR and solid-state NMR.

Figure 7b shows the Py-IR spectra of CZ-5 after pyridine adsorption followed by vacuum desorption at different temperatures. IR bands at 1545 and 1456 cm^{-1} are assigned to the Brønsted (B) and Lewis (L) acid sites, respectively. The obvious adsorption band at 1489 cm^{-1} is attributed to the vibration of the pyridine ring on both B and L acid sites.[30] As can be seen, all peak areas decrease with increasing the adsorption temperature, indicating that CZ-5 is a weak acid-dominant material. The B/L ratios range from 1.5 to 2.5 (Table S1, determined based on the intensity of these bands) at the three desorption temperatures, indicating that B acid dominates the acid sites. Both B and L acid sites can catalyze the cracking reaction, but strong L acid sites could accelerate the coking reaction.[31,32]

The coordination environment of Al in CZ-5 was also analyzed by ^{27}Al MAS NMR. As shown in Figure 8a, two significant peaks could be observed at 54 and 0 ppm; these peaks, respectively, belong to Al in a tetrahedral coordination framework (FAL) and Al in an octahedral coordination extra framework. A small peak was observed at 27 ppm, which indicates the presence of some five-coordinated extra-framework aluminosilicate phases.[33] The existence of framework Al and extra-framework Al indicates the formation of B and L acidic sites in the zeolite. The larger peak area at 54 ppm suggests that chainlike ZSM-5 is a B acid-dominant zeolite. The peak corresponding to FAL deconvolutes into five peaks centered at 52, 53, 54, 56, and 58 ppm (Figure 8b). The peak centered at 54 ppm corresponds to Al sites located at the intersection of the straight and zigzagged channels of ZSM-5, while the peak centered at 56 ppm corresponds to Al sites located within either the straight or zigzagged channels.[34,35] The peak area at 54 ppm (55.5%) was higher than that at 56

https://doi.org/10.1021/acsomega.2c05763
ACS Omega 2022, 7, 40520−40531

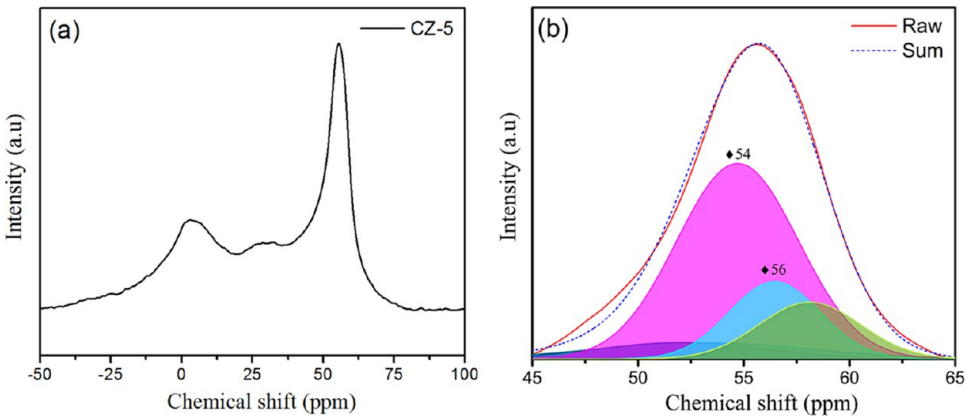

Figure 8. (a) ^{27}Al MAS NMR spectra and (b) individual Gaussian bands of CZ-5 in the chemical shift range from 45 to 65 ppm.

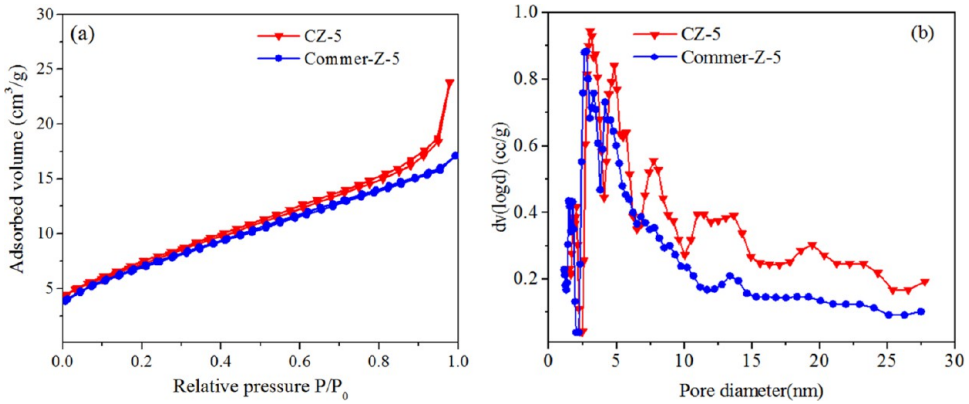

Figure 9. N_2 adsorption−desorption isotherms (a) and pore size distributions (b) of CZ-5 and Commer-Z-5 zeolites.

Table 2. Textural Properties of CZ-5 and Commer-Z-5

catalysts	S_{BET} (m^2/g)	S_{ext} (m^2/g)	D_{aver} (nm)	V_{total} (cm^3/g)	V_{micro} (cm^3/g)	V_{meso} (cm^3/g)	V_{meso}/V_{total}
CZ-5	538.7	488.5	5.72	0.77	0.025	0.744	0.97
Commer-Z-5	528.7	415.8	3.77	0.50	0.10	0.50	0.80

ppm (16.4%), which indicates that more Al is distributed at the junction of the straight and zigzagged channels in the skeleton structure. Such an Al distribution could help feedstock molecules access the acid sites of the zeolites.

Recent research showed that ^{31}P probe-assisted NMR (trimethylphosphine is commonly adopted as a probe molecule) is a reliable method to investigate the acidic features, namely, the type, concentration, and strength of acid sites for zeolite catalysts due to several advantages including the nearly 100% natural abundance of the ^{31}P nucleus and wide and defined chemical shift ranges.[36] This technique will be applied to further study the acidity of CZ-5 in future work.

3.2.3. Pore Structure. The N_2 adsorption−desorption isotherms and pore size distribution of CZ-5 are illustrated in Figure 9a and compared with those of Commer-Z-5. Commer-Z-5 revealed a typical type-I isotherm without any hysteresis loop even at high relative pressures, which means that the zeolite is microporous in nature. By comparison, the N_2 amount adsorbed by CZ-5 was much higher, and a type-II isotherm with a small hysteresis loop at a high relative pressure (P/P_0 = 0.5−0.99) was observed. These features indicate the presence of mesopores in CZ-5.[37] These mesopores can be attributed to the slit pores and/or intracrystal mesopores. Figure 9b shows the pore size distributions of the two ZSM-5 samples. Both zeolites showed a wide pore distribution of 1−27 nm, with the main pores concentrated at 3−6 nm. Table 2 summarizes the textural properties of the two ZSM-5 samples. Both samples showed a high specific surface area (>500 m^2/g). Compared with those of Commer-Z-5, the S_{BET}, S_{ext}, V_{total}, V_{meso}, D_{aver}, and V_{meso}/V_{total} ratio of CZ-5 significantly increased. The formation of mesopores in CZ-5 could be attributed to the following roles of PDDA: (i) PDDA aggregates act as a solid template for mesopores and (ii) PDDA-induced three-dimensional chain structures could generate intracrystal mesopores.[38] The presence of mesopores in CZ-5 promotes mass transfer and allows feedstock molecules to access the active sites on the zeolite easily.

3.3. Formation Mechanism of the Chainlike Structure. Semifinished particles generated during the crystallization process were collected every 4 h, and their morphologies were observed by SEM to clarify the growth mechanism of the zeolite. The ζ potentials of the synthesis mixture at different crystallization times were also determined.

As shown in Figure 10, a small number of short chains appeared following crystallization for 4 h; the number of short chains generated gradually increased with increasing crystallization time. Long and cross-linked chains were formed at crystallization times exceeding 24 h and increased with further

https://doi.org/10.1021/acsomega.2c05763
ACS Omega 2022, 7, 40520−40531

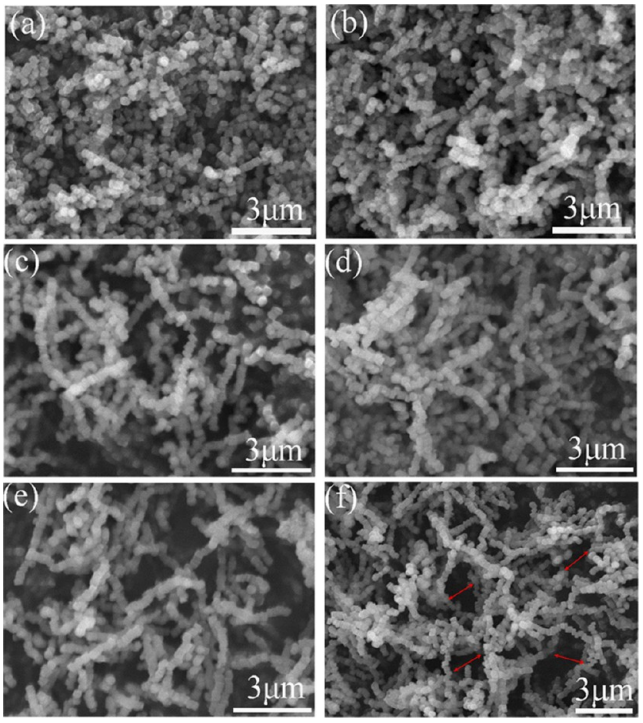

Figure 10. SEM images of ZSM-5 obtained at different crystallization times: (a) 4 h, (b) 16 h, (c) 24 h, (d) 32 h, (e) 40 h, and (f) 48 h.

increases in reaction time. As shown in Figure 11, the ζ potential of the synthesis mixture gradually decreased with

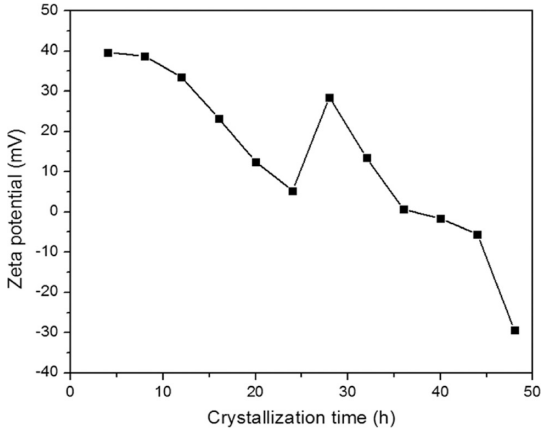

Figure 11. ζ Potential of the synthesis mixture at different crystallization times.

increasing crystallization time. As the ζ potential approached zero (reaction time, 24 h), the PDDA molecules and semifinished particles agglomerated under the action of van der Waals forces, which led to the formation of long chains and cross-linked chain structures.[38,39] A lot of macropores with pore sizes of about 1−2 μm appeared between the cross-linked chains (as indicated by red arrows in Figure 10f), which maybe result from the hard templating role of PDDA agglomerates.

The hydrolysis of TEOS produces weakly acidic silanol, which tends to transfer into the strong alkaline SiO^- under alkaline conditions. The formation of more negatively charged groups leads to the gradual decrease of the ζ potential of crystallization solution during the initial 24 h (even though these SiO^- groups could be consumed via the polymerization reaction). Subsequently, a temporary increase in the ζ potential was observed at 30 h, which could be related to the crystallization degree. During this period, the crystallization reaction of the most negatively charged Si(Al)−O^- groups has been completed (i.e., Si−O^- and Al−O^- groups have been transformed into Si−O−Si(Al)), and thus, the consumption of negatively charged groups lead to a temporary increase of ζ potential. After 30 h, the formed zeolite framework could be corroded when exposed to alkaline conditions for a long time and release some negatively charged Si(Al)−O^- groups again, consequently leading to the gradual decrease of ζ potential.[37]

The mean particle size in the synthesis mixture was measured by DLS at different times to confirm the roles of PDDA (Figure S3). The mean particle size prior to the addition of TEOS was 3.6 μm. The particle size then increased to ∼7.0 μm with the addition TEOS for 7 h and subsequently decreased to 2.5 μm with the addition of TEOS for 24 h. This trend illustrates that PDDA exists as aggregates consisting of dozens of molecules.[21] Thus, combined with the above results, we propose the formation mechanism of the chainlike zeolite shown in Scheme 1. The negatively charged aluminosilicate precursors (i.e., Si−OH, Al−OH) are initially attracted to the positively charged PDDA aggregates, which leads to a decrease in ζ potential. The aluminosilicate species then nucleate under the structure-directing role of TPAOH (as shown in Figures 1 and 2), and the crystal nuclei continue to grow by consuming Si−OH and Al−OH. Soluble PDDA/aluminosilicate electrostatic conjugates are absorbed onto the (010) crystal faces of the developing zeolites, which reduces the surface energy and presents reactive species (e.g., Si−OH, Al−OH). Neighboring crystals are closely connected along their *b*-axis via the condensation of surface hydroxyl groups between crystals. Following extended crystallization (e.g., 24 h), the decrease in the surface charge of the sol particles causes the agglomeration of PDDA molecules and short-chain semifinished particles,

Scheme 1. Formation Mechanism of the Chainlike ZSM-5 Zeolite

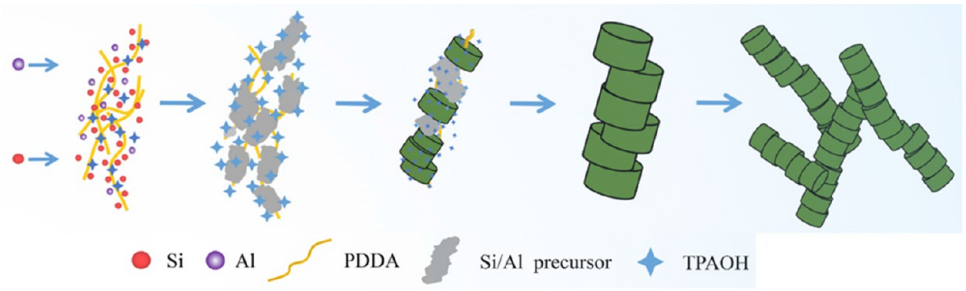

https://doi.org/10.1021/acsomega.2c05763
ACS Omega 2022, 7, 40520−40531

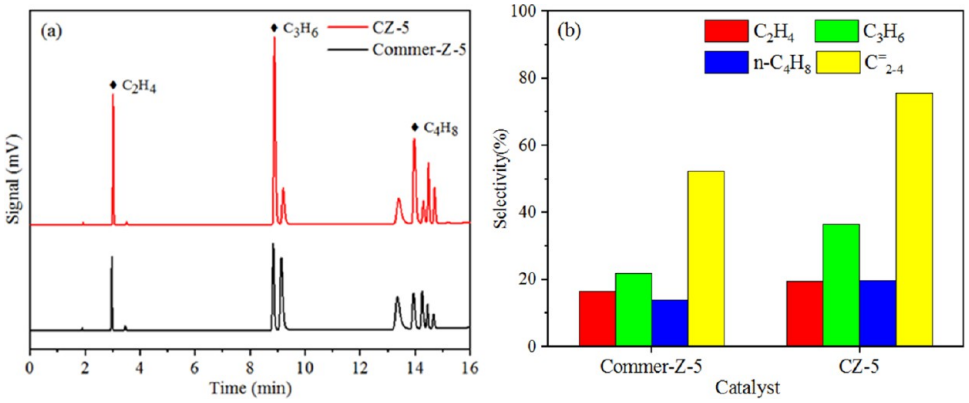

Figure 12. GC of gas products from the catalytic cracking of oleic acid (a) and selectivity of light olefins (b).

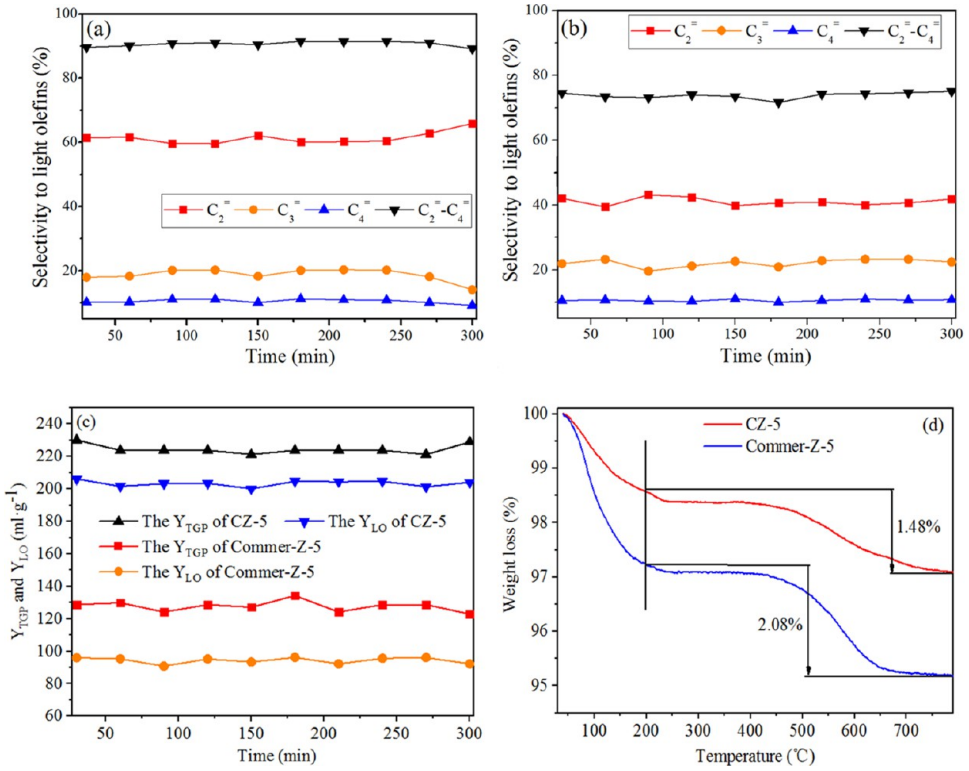

Figure 13. Selectivity to light olefins from the catalytic cracking of ethanol over (a) CZ-5 and (b) Commer-Z-5; (c) the total gas yield and light olefin yield of the two zeolites; and (d) TGA profiles of the used catalysts.

which leads to the formation of long chains and cross-linked chain structures via van der Waals forces. The formation of chainlike zeolites could be ascribed to the synergistic action between PDDA and TPAOH. TPAOH plays multiple roles in the reaction system; it dissolves the aluminosilicate gel, induces nucleation, controls the particle size of individual crystals, and stacks the adjacent crystals. PDDA agglomerates act both as a soft templating agent to attract negatively charged Si(Al)−OH toward the PDDA agglomerates to induce nucleation via electrostatic attraction and as a hard templating agent to form three-dimensional mesoporous structures.

3.4. Catalytic Cracking Tests. Figure 12 shows the GC spectra of gas products obtained from the catalytic cracking of oleic acid over CZ-5 and Commer-Z-5. The selectivities of CZ-5 for light olefins ($C_{2-4}^{=}$) and propylene were 75.7 and 36.5%, respectively; these values are much higher than those of Commer-Z-5 (52.3 and 21.9%, respectively). The Y_{TGP} and Y_{LO} of CZ-5 were 119 and 90 mL/g, respectively, which are also much higher than those of Commer-Z-5 (55 and 29 mL/g, respectively). These results show that the synthesized chainlike ZSM-5 is superior to commercial ZSM-5 for light olefin production. The superior catalytic performance is related to the mild acidity and three-level porous structure (macropores in cross-linked chains, intracrystal mesopores, and intracrystal micropores). CZ-5 possessed mild acidity (mainly including B acidic sites and a small amount of L acidic sites), which helps appropriate cracking and deoxygenation reactions of oleic acid while preventing excessive secondary reactions, e.g., further cracking, hydrogen transfer, and aromatization to produce undesired products, e.g., light alkanes, polycyclic aromatics, and coke. The L acid sites in the zeolite could contribute to the deoxygenation of oleic acid. The macropores in cross-linked chains allow the feedstock molecules to rapidly reach the surface of the chains and preliminarily decompose,

https://doi.org/10.1021/acsomega.2c05763
ACS Omega 2022, 7, 40520−40531

and the decomposed intermediates then diffuse into the chains through zigzag channels and intracrystal mesopores, consequently causing a shape-selective catalysis reaction on the active sites in the channels. The long straight channels in the *b*-axis direction probably help to increase the residence time of the cracked intermediates and thus improve the formation of light olefins. Commer-Z-5 possesses a large number of strong acid sites and a microporous structure, which are liable to cause rapid cracking and hydrogen transfer reactions on the surface of the catalyst, consequently leading to the formation of coke and a decrease in catalytic performance.

Figure 13 shows the results of the catalytic cracking of ethanol to produce light olefins over CZ-5. After continuous cracking for 300 min, the light olefin selectivities of CZ-5 and Commer-Z-5 remained at approximately 90 and 75%, respectively. The ethylene selectivity of CZ-5 reached 60%, which is 20% higher than that of Commer-Z-5. Moreover, the Y_{TGP} and Y_{LO} of CZ-5 were 230 and 207 mL/g, respectively, which are much higher than those of Commer-Z-5 (130 and 90 mL/g, respectively). These results indicate that the synthesized chainlike zeolite has excellent hydrothermal stability and is an ideal catalyst for the production of light olefins.

The TG profiles of spent CZ-5 and Commer-Z-5 are shown in Figure 13d. The weight loss at 200−800 °C is mainly due to the oxidation of coke.[40] Spent CZ-5 showed less weight loss than Commer-Z-5 at 200−800 °C, which indicates that lower amounts of coke are deposited on CZ-5. The mild acidity and mesoporous structure of CZ-5 could help restrain coking and, thus, prolong the lifetime of the catalyst.[41]

In one of our previous studies, mesoporous ZSM-5 (SiO_2/Al_2O_3 = 200) was synthesized with a conventional hydrothermal method, in which TPAOH and CTAB were used as dual templates, aiming to increase the pore size and reduce the mass transfer resistance of large molecules in zeolites. The resultant ZSM-5 achieved a light olefin selectivity of 45% from ethanol and 26% from oleic acid cracking at 400 °C in a N_2 atmosphere.[42] The selectivities were further improved to 80% (for ethanol) and 60% (for oleic acid) by the cracking of the feeds in a steam atmosphere.[43] The light olefin selectivities from ethanol (90%) and oleic acid (75.7%) cracking over the present chainlike ZSM-5 are always higher than those from the previously synthesized mesoporous ZSM-5 whether cracking in steam or N_2 stream, demonstrating the superior shape-selective catalysis capability of the present ZSM-5. The mild acidity and the presence of the distinctive three-level porous structure (macropores in cross-linked chains, intracrystal mesopores, and long straight channels in the *b*-axis direction in chains) would act synergistically in improving mass transfer, promoting cracking, and suppressing coking, consequently leading to the selective formation of light olefins.

4. CONCLUSIONS

The appropriate parameters for the synthesis of chainlike ZSM-5 in the presence of PDDA and TPAOH were investigated. The optimized composition of the synthesis mixture is as follows: TEOS as the silicon source, ANI as the aluminum source, and PDDA/SiO_2, TPAOH/SiO_2, SiO_2/Al_2O_3, and H_2O/SiO_2 ratios of 0.16, 0.4, 50, and 40, respectively. Crystallization should be carried out at 180 °C for over 24 h. The formation of chainlike zeolites was attributed to the synergistic action between PDDA and TPAOH. TPAOH played an important role in inducing the formation of single crystals with the proper dimensions and flat surfaces by precisely controlling the hydrolysis rate of the silicon/aluminum sources. PDDA acted as a soft template to encourage negatively charged Si(Al)−OH to assemble around PDDA agglomerates, thus promoting nucleation; it also functioned as a hard template to form three-dimensional mesoporous structures. The condensation of surface hydroxyl groups on the (010) faces of the crystals resulted in the tight cross-linking of adjacent crystals. The resultant zeolites showed mild acidity, three-dimensional mesoporous structures, and superior catalytic performance in converting oleic acid and ethanol to light olefins.

■ ASSOCIATED CONTENT

Supporting Information

The Supporting Information is available free of charge at https://pubs.acs.org/doi/10.1021/acsomega.2c05763.

SEM images of the zeolites obtained from different types of silicon sources and aluminum sources; dynamic light scattering (DLS) data of precursor mixtures with the addition of TEOS for different times; and quantitative analysis of the types of acid sites of the zeolite (PDF)

■ AUTHOR INFORMATION

Corresponding Author

Zhixia Li − *School of Chemistry and Chemical Engineering, Guangxi University, Nanning 530004 Guangxi, China;* orcid.org/0000-0001-8834-4649; Phone: +86-771-3233718; Email: zhixiali@gxu.edu.cn

Authors

Wen He − *School of Chemistry and Chemical Engineering, Guangxi University, Nanning 530004 Guangxi, China*

Fuwei Li − *School of Chemistry and Chemical Engineering, Guangxi University, Nanning 530004 Guangxi, China*

Yufei Gu − *School of Chemistry and Chemical Engineering, Guangxi University, Nanning 530004 Guangxi, China*

Xiaofeng Wang − *School of Chemistry and Chemical Engineering, Guangxi University, Nanning 530004 Guangxi, China*

Hengshuo Gu − *School of Chemistry and Chemical Engineering, Guangxi University, Nanning 530004 Guangxi, China*

Hongbing Fu − *School of Chemistry and Chemical Engineering, Guangxi University, Nanning 530004 Guangxi, China*

Xiumei Liang − *School of Chemistry and Chemical Engineering, Guangxi University, Nanning 530004 Guangxi, China*

Complete contact information is available at: https://pubs.acs.org/10.1021/acsomega.2c05763

Notes

The authors declare no competing financial interest.

■ ACKNOWLEDGMENTS

The authors are grateful for support from the National Natural Science Foundation of China (22078076), the Guangxi Natural Science Foundation (2020GXNSFAA159174), and the Opening Project of National Enterprise Technology Center of Guangxi Bossco Environmental Protection Technology Co., Ltd (GXU-BFY-2020-005).

REFERENCES

(1) Ye, Z.; Zhao, Y.; Zhang, H.; Zhang, Y.; Tang, Y. Co-hydrolysis and seed-induced synthesis of basic mesoporous ZSM-5 zeolites with enhanced catalytic performance. *Chem. - Eur. J.* **2020**, *26*, 6147−6157.
(2) Sebestyén, Z.; Barta-Rajnai, E.; Bozi, J.; Blazsó, M.; Jakab, E.; Miskolczi, N.; Sója, J.; Czégény, Z. Thermo-catalytic pyrolysis of biomass and plastic mixtures using HZSM-5. *Appl. Energy* **2017**, *207*, 114−122.
(3) Kaerger, J. Random walk through two-channel networks: a simple means to correlate the coefficients of anisotropic diffusion in ZSM-5 type zeolites. *J. Phys. Chem. A* **1991**, *95*, 5558−5560.
(4) Caro, J.; Noack, M.; Richter-Mendau, J.; Marlow, F.; Petersohn, D.; Griepentrog, M.; Kornatowski, J. Selective sorption uptake kinetics of n-hexane on ZSM-5-A new method for measuring anisotropic diffusivities. *J. Phys. Chem. A* **1993**, *97*, 13685−13690.
(5) Díaz, I.; Kokkoli, E.; Terasaki, O.; Tsapatsis, M. Surface structure of zeolite (MFI) crystal. *Chem. Mater.* **2004**, *16*, 5226−5232.
(6) Li, S.; Li, J.; Dong, M.; Fan, S.; Zhao, T.; Wang, J.; Fan, W. Strategies to control zeolite particle morphology. *Chem. Soc. Rev.* **2019**, *48*, 885−907.
(7) Hartmann, M.; Gonche, M. A.; Schwieger, W. Catalytic test reactions for the evaluation of hierarchical zeolites. *Chem. Soc. Rev.* **2016**, *45*, 3313−3330.
(8) Xin, H. Novel Carbon-templating procedure for synthesis of mesoporous Fe/ZSM-5 with enhanced performance in hydroxylation of benzene with nitrous oxide. *Energy Environ. Focus* **2014**, *3*, 297−308.
(9) Čejka, J.; Mintova, S. Perspectives of micro/mesoporous composites in catalysis. *Catal. Rev.* **2007**, *49*, 457−509.
(10) Beck, J. S.; Vartuli, J. C.; Roth, W. J.; Leonowicz, M. E.; Kresge, C. T.; Schmitt, K. D.; Chu, C. T. W.; Olson, D. H.; Sheppard, E. W.; McCullen, S. B.; Higgins, J. B.; Schlenker, J. L. A new family of mesoporous molecular sieve prepared with liquid crystal templates. *J. Am. Chem. Soc.* **1992**, *114*, 10834−10843.
(11) Yu, Q.; Meng, X.; Liu, J.; Li, C.; Cui, Q. A fast organic template-free, ZSM-11 seed-assisted synthesis of ZSM-5 with good performance in methanol-to-olefin. *Microporous Mesoporous Mater.* **2013**, *181*, 192−200.
(12) Aoki, K.; Mann, S. Polyelectrolyte-mediated synthesis and self-assembly of silicalite nanocrystals into linear chain superstructures. *J. Mater. Chem.* **2005**, *15*, 111−113.
(13) Wang, R.; Liu, W.; Ding, S.; Zhang, Z.; Li, J.; Qiu, S. Mesoporous MFI zeolites with self-stacked morphology templated by cationic polymer. *Chem. Commun.* **2010**, *46*, 7418−7420.
(14) Jin, L.; Xie, T.; Liu, S.; Li, Y.; Hu, H. Controllable synthesis of chainlike hierarchical ZSM-5 templated by ducrose and its catalytic performance. *Catal. Commun.* **2016**, *75*, 32−36.
(15) Jiang, J.; Ji, S.; Duanmu, C.; Pan, Y.; Wu, J.; Wu, M.; Chen, J. Self-assembly of fibrous ZSM-5 zeolites in the presence of sodium Alginate. *Particuology* **2017**, *33*, 55−62.
(16) Quan, Y.; Li, S.; Wang, S.; Li, Z.; Dong, M.; Qin, Z.; Chen, G.; Wei, Z.; Fan, W.; Wang, J. Synthesis of chainlike ZSM-5 zeolites: determination of synthesis parameters, mechanism of chainlike morphology formation, and their performance in selective adsorption of xylene isomers. *ACS Appl. Mater. Interface* **2017**, *9*, 14899−14910.
(17) Ma, X.; Li, G.; Tao, J.; Li, P.; Zheng, H.; Li, S.; Xu, Y. Synergistic chemical synthesis and self-assembly lead to three-dimensional b-oriented MFI superstructures with selective adsorption and luminescenceproperties. *Chem. - Eur. J.* **2018**, *24*, 2980−2986.
(18) Song, W.; Justice, R. E.; Jones, C. A.; Grassian, V. H.; Larsen, S. C. Synthesis, characterization, and adsorption properties of nano-crystalline ZSM-5. *Langmuir* **2004**, *20*, 8301−8306.
(19) Dubas, S. T.; Schlenoff, J. Factors controlling the growth of polyelectrolyte multilayers. *Macromolecules* **1999**, *32*, 8153−8160.
(20) Li, F.; Ding, S.; Wang, Z.; Li, Z.; Li, L.; Gao, C.; Zhong, Z.; Lin, H.; Chen, C. Production of light olefins from catalytic cracking bio-oil model compounds over La_2O_3-modified ZSM-5 zeolite. *Energy Fuels* **2018**, *32*, 5910−5922.
(21) Dobrynin, A. V.; Rubinstein, M. Adsorption of hydrophobic polyelectrolytes at oppositely charged surfaces. *Macromolecules* **2002**, *35*, 2754−2768.
(22) Brar, T.; France, P.; Smirniotis, P. Control of crystal size and distribution of zeolite A. *Ind. Eng. Chem. Res.* **2001**, *40*, 1133−1139.
(23) Wang, K.; Karlsson, G.; Almgren, M. Aggregation behavior of cationic fluorosurfactants in water and salt solutions. A CryoTEM survey. *J. Phys. Chem. B* **1999**, *103*, 9237−9246.
(24) Mochizuki, H.; Yokoi, T.; Imai, H.; Watanabe, R.; Namba, S.; Kondo, J. N.; Tatsumi, T. Facile control of crystallite size of ZSM-5 catalyst for cracking of hexane. *Microporous Mesoporous Mater.* **2011**, *145*, 165−171.
(25) Sashkina, K. A.; Qi, Z.; Wu, W.; Ayupov, A. B.; Lysikov, A. I.; Parkhomchuk, E. V. The effect of H_2O/SiO_2 ratio in precursor solution on the crystal size and morphology of zeolite ZSM-5. *Microporous Mesoporous Mater.* **2017**, *244*, 93−100.
(26) Cundy, C. S.; Cox, P. A. The hydrothermal synthesis of zeolites: history and development from the earliest days to the present time. *Chem. Rev.* **2003**, *103*, 663−701.
(27) Penn, R. L.; Banfield, J. F. Imperfect oriented attachment: dislocation generation in defect-free nanocrystals. *Science* **1998**, *281*, 969−971.
(28) Xing, A.; Zhang, N.; Yuan, D.; Liu, H.; Sang, Y.; Miao, P.; Sun, Q.; Luo, M. Relationship between acidity, defective sites, and diffusion properties of nanosheet ZSM-5 and its catalytic performance in the methanol to propylene reaction. *Ind. Eng. Chem. Res.* **2019**, *58*, 12506−12515.
(29) Gorte, R. J.; Crossley, S. P. A perspective on catalysis in solid acids. *J. Catal.* **2019**, *375*, 524−530.
(30) Yaripour, F.; Shariatinia, Z.; Sahebdelfar, S.; Irandoukht, A. Conventional hydrothermal synthesis of nanostructured H-ZSM-5 catalysts using various templates for light olefins production from methanol. *J. Nat. Gas Sci. Eng.* **2015**, *22*, 260−269.
(31) Li, D.; Tan, Z.; Zhang, H.; Zheng, Y. Influence of the acidity and pore structure of FCC catalysts on coke selectivity. *Ind. Catal.* **2013**, *21*, 49−52.
(32) Jin, Y. S.; Wang, Y. S.; Wang, L.; Sun, S.; Guo, Y.; Guo, Y. L.; Lu, G. Z. The study of γ-Al_2O_3 modified by halogen and its application in MTBE cracking. *Appl. Chem. Ind.* **2017**, *46*, 2150−2157.
(33) Triantafyllidis, K. S.; Nalbandian, L.; Trikalitis, P. N.; Ladavos, A. K.; Mavromoustakos, T.; Nicolaides, C. P. Compositional and acidic characteristics of nanosized amorphous or partially crystalline ZSM-5 zeolite-based materials. *Microporous Mesoporous Mater.* **2004**, *75*, 89−100.
(34) Kim, S.; Park, G.; Woo, M. H.; Kwak, G.; Kim, S. K. Control of hierarchical structure and framework-Al distribution of ZSM-5 via adjusting crystallization temperature and their effects on methanol conversion. *ACS Catal.* **2019**, *9*, 2880−2892.
(35) Wang, S.; Wang, P.; Qin, Z.; Chen, Y.; Dong, M.; Li, J.; Zhang, K.; Liu, P.; Wang, J.; Fan, W. Relation of catalytic performance to the aluminum siting of acidic zeolites in the conversion of methanol to olefins, viewed via a comparison between ZSM-5 and ZSM-11. *ACS Catal.* **2018**, *8*, 5485−5505.
(36) Peng, Y. K.; Tsang, S. C. E. Probe-assisted NMR: Recent progress on the surface study of crystalline metal oxides with various terminated facets. *Magn. Reson. Lett.* **2022**, *2*, 9−16.
(37) Wang, L.; Zhang, Z.; Yin, C.; Shan, Z.; Xiao, F. S. Hierarchical mesoporous zeolites with controllable mesoporosity templated from cationic polymers. *Microporous Mesoporous Mater.* **2010**, *131*, 58−67.
(38) Du, L.; Kong, F.; Chen, G.; Du, C.; Gao, Y.; Yin, G. A review of applications of poly(diallyldimethyl ammonium chloride) in polymer membrane fuel cells: from nanoparticles to support materials. *Chin. J. Catal.* **2016**, *37*, 1025−1036.
(39) Lupulescu, A. I.; Rimer, J. D. In situ imaging of silicalite-1 surface growth reveals the mechanism of crystallization. *Science* **2014**, *344*, 729−732.
(40) Castaño, P.; Elordi, G.; Olazar, M.; Aguayoa, A. T.; Pawelec, B.; Bilbao, J. Insights into the coke deposited on HZSM-5, Hβ and HY

https://doi.org/10.1021/acsomega.2c05763
ACS Omega 2022, 7, 40520−40531

zeolites during the cracking of polyethylene. *Appl. Catal. B* **2011**, *104*, 91−100.
(41) Shamzhy, M.; Opanasenko, M.; Concepción, P.; Martínez, A. New trends in tailoring active sites in zeolite-based catalysts. *Chem. Soc. Rev.* **2019**, *48*, 1095−1149.
(42) Zhao, T.; Li, F.; Yu, H.; Ding, S.; Li, Z.; Huang, X.; Li, X.; Wei, X.; Wang, Z.; Lin, H. Synthesis of mesoporous ZSM-5 zeolites and catalytic cracking of ethanol and oleic acid into light olefins. *Appl. Catal., A* **2019**, *575*, 101−110.
(43) Li, Z.; Li, F.; Zhao, T.; Yu, H.; Ding, S.; He, W.; Song, C.; Zhang, Y.; Lin, H. The effect of steam on maximizing light olefin production by cracking of ethanol and oleic acid over mesoporous ZSM-5 catalysts. *Catal. Sci. Technol.* **2020**, *10*, 6618−6627.

https://doi.org/10.1021/acsomega.2c05763
ACS Omega 2022, 7, 40520−40531